UNIVERSITY OF ALBERTA

Dynamics of Energetic Electrons in a Microinjection Event.

Ji Liu[1], Robert Rankin[1], Alex W. Degeling[2] and F. Fenrich[1]

[1]University of Alberta, Edmonton, Canada.

[2]Shandong University, Weihai, China.

Outline

- A simplified analytical model of ULF toroidal mode waves is presented
- The model includes the transient growth and damping of ULF waves, including phase mixing on the background magnetic field.
- The model is applied to investigate drift-resonant dynamics of electrons with ULF waves, and the associated modulation on the electron flux.

Introduction

➢ ULF waves and wave-particle interactions

- Wave-particle interactions involving ultra-low-frequency (ULF) waves are of significance in space physics due to their role in the energization and transport of charged particles [*Zong et al., Rev. Mod. Plasma Phys., 2017*].
- Standing ULF waves are classified as toroidal and poloidal modes, which can be excited by interplanetary shocks, solar wind dynamic pressure pulses, and other processes [*Zong et al., JGR, 2009; Wang et al., JGR, 2018; Degeling et al., JGR, 2020*].
- Toroidal mode drift resonance with electrons is less studied because of its perceived lower acceleration efficiency. Recently, Li et al. (*2021*, *JGR*) reported toroidal mode electron drift-resonance in which the magnetic field developed a compressional component.
- Here, we extend the work of Li et al. (2021, JGR) through the development of a simplified model of ULF waves and test-particle guiding center simulations.

➢ Microinjections

- Microinjections in Earth's magnetosphere exhibit a repetitive dispersive electron signature that appears similar to substorm-associated injections.
- Sarafopoulos (*2002*, *GRL*) postulated the existence of a sharp and meandering electron injection boundary near geosynchronous orbit that supplies energetic electrons observed as pulsating injections into the earthward region.

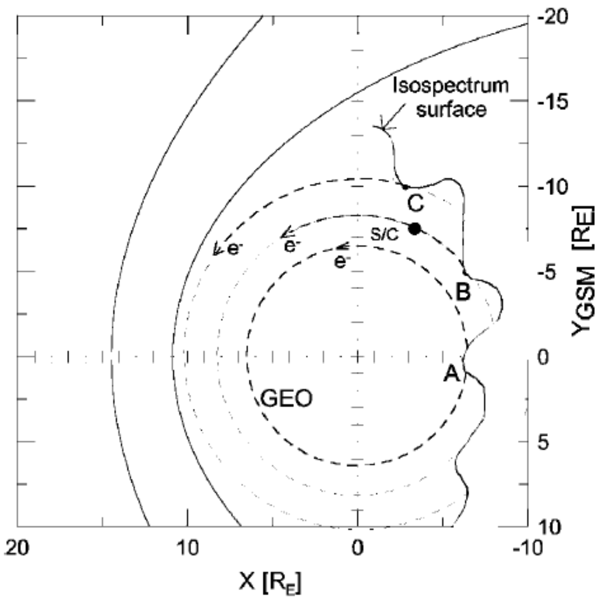

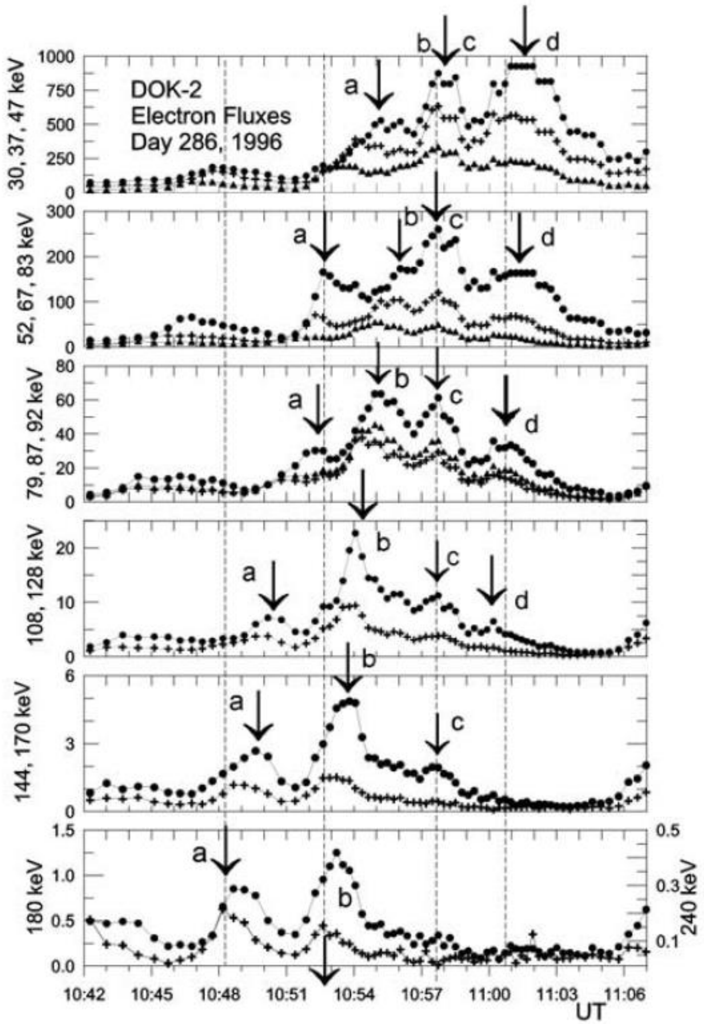

(*Sarafopoulos, Geophys. Res. Lett., 2002*)

➢ Microinjection and ULF waves

- MMS (Magnetospheric Multi Scale) satellite observations in the pre-midnight magnetosphere at L≳ 9 [Fennell et al., *2016, GRL*] show similar dispersive electron signatures associated with Ultralow-frequency (ULF) waves but without substorms.

- In these microinjection events:

a) The electron residual flux has a maximum at the expected resonant energy.

b) The observed modulations in the residual electron flux exhibit a 180° phase change with energy.

c) The phase at high energy lags the phase at low energy, which is consistent with that expected of toroidal mode drift-resonant interaction.

d) The peaks and valleys of the toroidal electric field are phase-correlated with the flux.

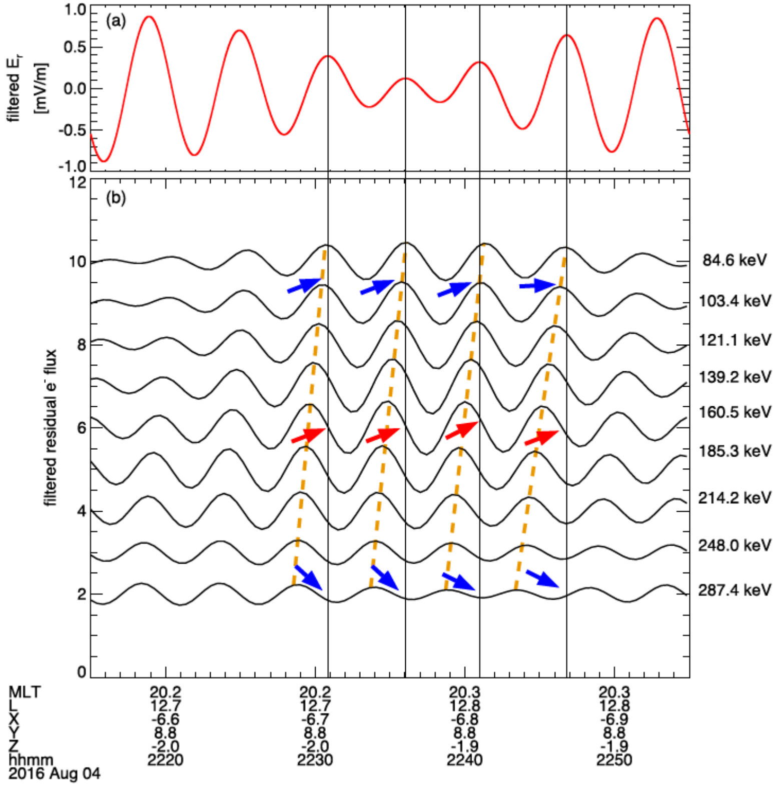

(*Luo et al., GRL, 2022*)

➢ ULF Waves and Microinjection

- Luo et al. (*2022*, *GRL*) suggested that drift-resonance between electrons and ULF toroidal waves may be interpreted as microinjections.

- Using drift-resonance theory, they explored phase differences in the residual flux observed at different energy channels during MMS microinjection events:

$$\delta j \propto \delta E_{tv} e^{-i(\psi+\pi)} = \delta E_v \exp i(m\phi - (\omega t + \psi + \pi))$$

$$\psi = \arg\left((m\omega_{d,b} - \omega_r) - i\omega_i\right)$$

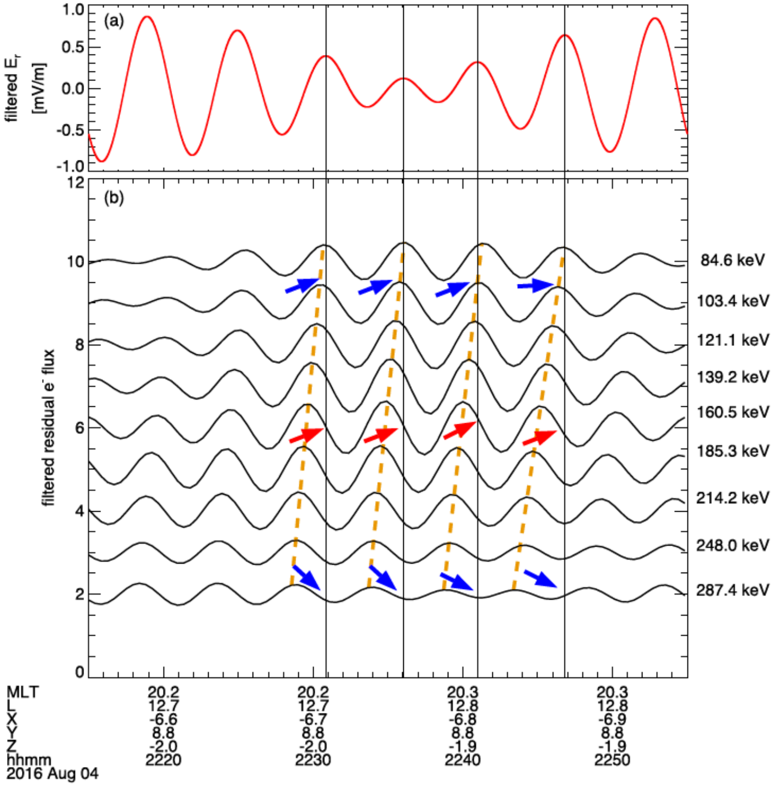

(*Luo et al., Geophys. Res. Lett., 2022*)

MMS observations

➢ **Energetic electron microinjections observed by MMS**

- We revisit the ULF wave microinjection event reported by (*Luo et al.*, *GRL*, *2022*).
- The ULF wave was dominantly toroidal between 22:00-23:00 UT on August 4th, 2016.
- Using data from the Magnetospheric Multiscale (MMS) mission:
  - ✓ f_{wave} ~3 mHz.
  - ✓ Maximum amplitude of residual flux at ~160.5 keV.
  - ✓ $m = \omega_{wave}/\omega_{drift} = 4$.

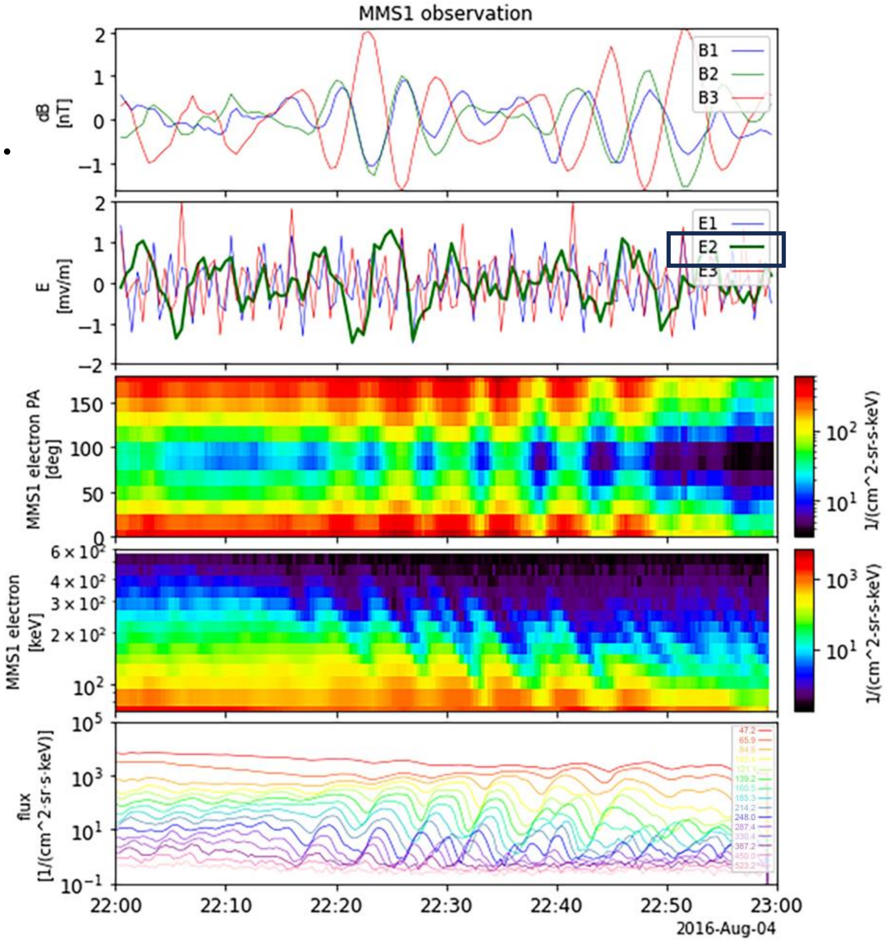

Dipole field approximation

➢ MMS position

✓ Original position: $L = 11.6, Lat = -20.4°, \emptyset = 120.9°$

- T96 geomagnetic model.
- The averaged solar wind condition during the event from Omni database: $D_p = 2.5\,nPa,\ B_y = 2.2nT, B_z = -3.0nT, V_{sw} = (-549,\ -17,\ 3)\ km/m, Dst = -16.0nT.$
- The same particle's dynamics along the magnetic field line:

$$\frac{B_{prob}^{T96}}{B_{prob}^{T96}} = \frac{B_{prob}^{dipole}}{B_{prob}^{dipole}}$$

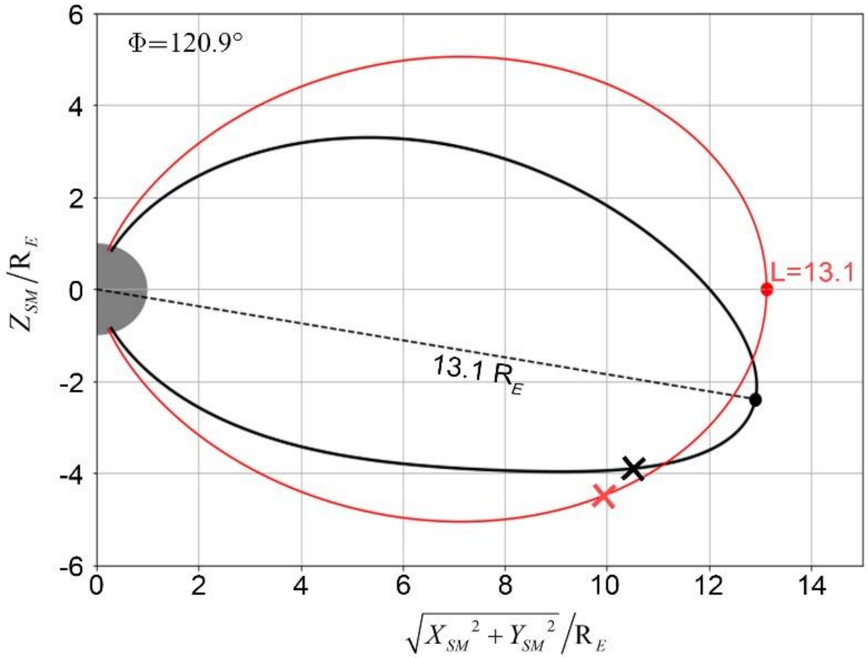

✓ Projected position: $L' = 13.61\ Lat' = -24.3°, \emptyset' = 120.9°$

MLT=20h

Analytical solution for the toroidal fundamental mode

E in the radial direction:

$$\Delta E_2 = \tilde{E}_{20}\frac{(\omega_0 L_0 R_E)^2}{h_2\Pi}\cos(f_N s)\cdot\left\{\left(\omega_N{}^2-\omega_0{}^2\right)\cos(\omega_0\tau)+\omega_0\gamma\sin(\omega_0\tau)-e^{-\frac{\gamma t}{2}}\left[\Lambda\cdot\cos(\Omega t)+\Sigma\cdot\sin(\Omega t)\right]\right\}$$

B in the azimuthal direction

$$\Delta B_3 = \tilde{E}_{20}\frac{(\omega_0 L_0 R_E)^2}{L^2 R_E{}^2 h_3\Pi} f_N\sin(f_N s)\cdot\left\{\begin{array}{l}\frac{\left(\omega_N{}^2-\omega_0{}^2\right)}{\omega_0}\sin(\omega_0\tau)-\gamma\cos(\omega_0\tau)\\ -\frac{1}{2\omega_N{}^2}e^{-\frac{\gamma t}{2}}\left[(2\Omega\Lambda-\gamma\Sigma)\sin(\Omega t)-(\gamma\Lambda+2\Omega\Sigma)\cos(\Omega t)\right]\end{array}\right\}$$

B in background field direction

$$\Delta B_1 = -\tilde{E}_{20} m\frac{(\omega_0 L_0 R_E)^2}{h_1\Pi}\cos(f_N s)\cdot\left\{\begin{array}{l}\frac{\left(\omega_N{}^2-\omega_0{}^2\right)}{\omega_0}\cos(\omega_0\tau)+\gamma\sin(\omega_0\tau)\\ +\left[\frac{\left(\gamma^2-2\omega_N{}^2+2\omega_0{}^2\right)}{2\Omega}\sin(m\Phi)-\frac{\gamma\left(\omega_N{}^2+\omega_0{}^2\right)}{2\Omega\omega_0}\cos(m\Phi)\right]\sin(\Omega t)e^{-\frac{\gamma t}{2}}\\ +\left[\gamma\sin(m\Phi)-\frac{\left(\omega_N{}^2-\omega_0{}^2\right)}{\omega_0}\cos(m\Phi)\right]\cos(\Omega t)e^{-\frac{\gamma t}{2}}\end{array}\right\}$$

Six paraments to reproduce the wave field.

1) Frequency of monochromatic driver: ω_0
2) Wave number in azimuthal direction: m
3) Resonance field line: L_0
4) Amplitude of E in the resonance point at the equator: $\tilde{E}_{20}$
5) Damping rate of waves: γ
6) The initial time: t_0

$$\left\{\begin{array}{ll}\tau = t-\frac{m\Phi}{\omega_0} & (3)\\ V_{A0} = \frac{2\omega_0 R_E}{\pi}\sqrt{L_0{}^2-L_0} & (4)\\ f_N = \frac{\pi}{2}\cdot\sqrt{\frac{L}{L-1}} & (5)\\ \omega_N = \frac{V_{A0} f_N}{r_{eq}} & (6)\end{array}\right.$$

➢ Reproduce the observed field by model.

For the other parameters including the specific L_0, amplitude $\tilde{E}_{20}$, damping rate γ and the initial time t_0, we manually adjusted them until the model results agreed with the observations.

ω_0 (mHz)	m	L_0	$\tilde{E}_{20}$ (mV/m)	γ (ω_0)	t_0 (s)
3.0	4	9.9	0.28	$\frac{1}{500}$	2016-08-04 21:58:00

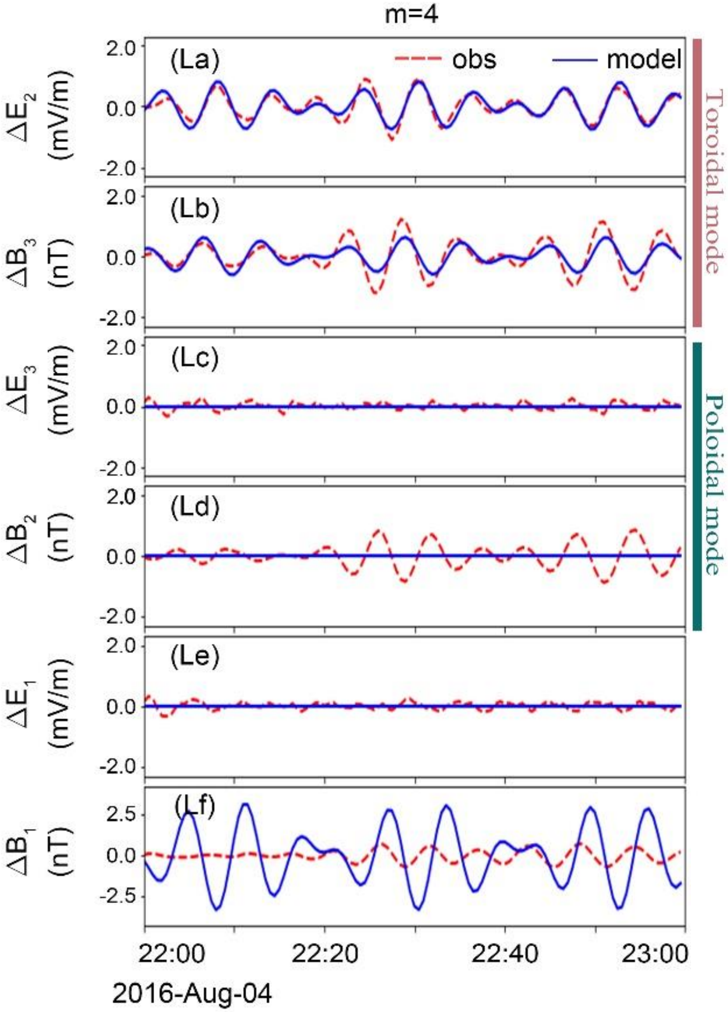

Observed and modeled toroidal waves exhibit a beat pattern, i.e., the wave envelope is fluctuating with time.

Reproduce the observation

➢ Reproduce the observed field by model.

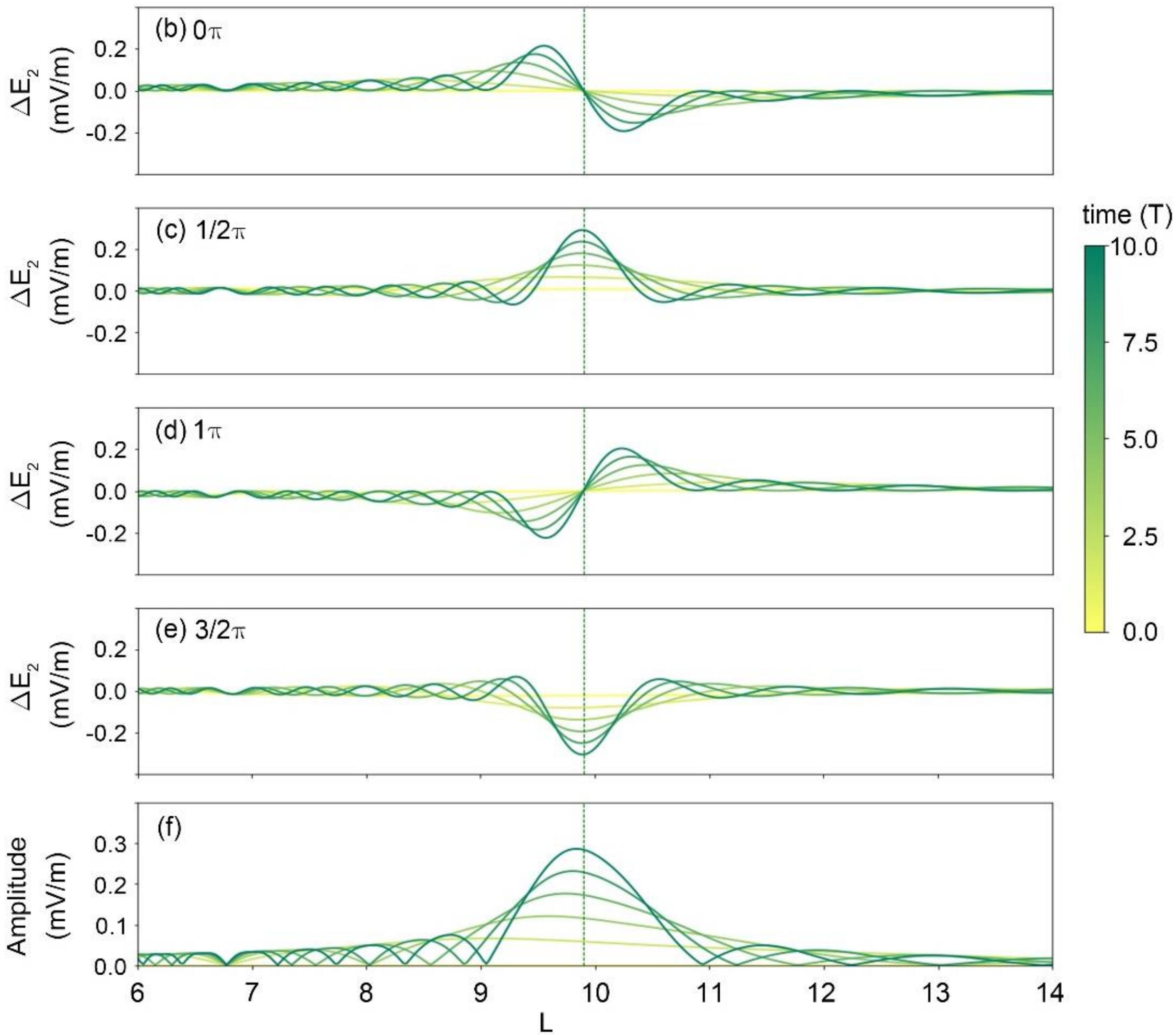

The corresponding amplitude distribution along the radial direction displays the well-known sinc function behavior of the wave amplitude, with a secular term $|t\,\mathrm{Sinc}(xt)|$ that is typical of linear driven resonant systems. Thus, at a fixed L different from L_0, secondary peaks and troughs of the electric field profile will appear and disappear as time increases. These characteristic features obtained from the modeling results correspond to phase mixing of the excited ULF toroidal mode wave.

Reproduce the the observation

➢ Phase Mixing

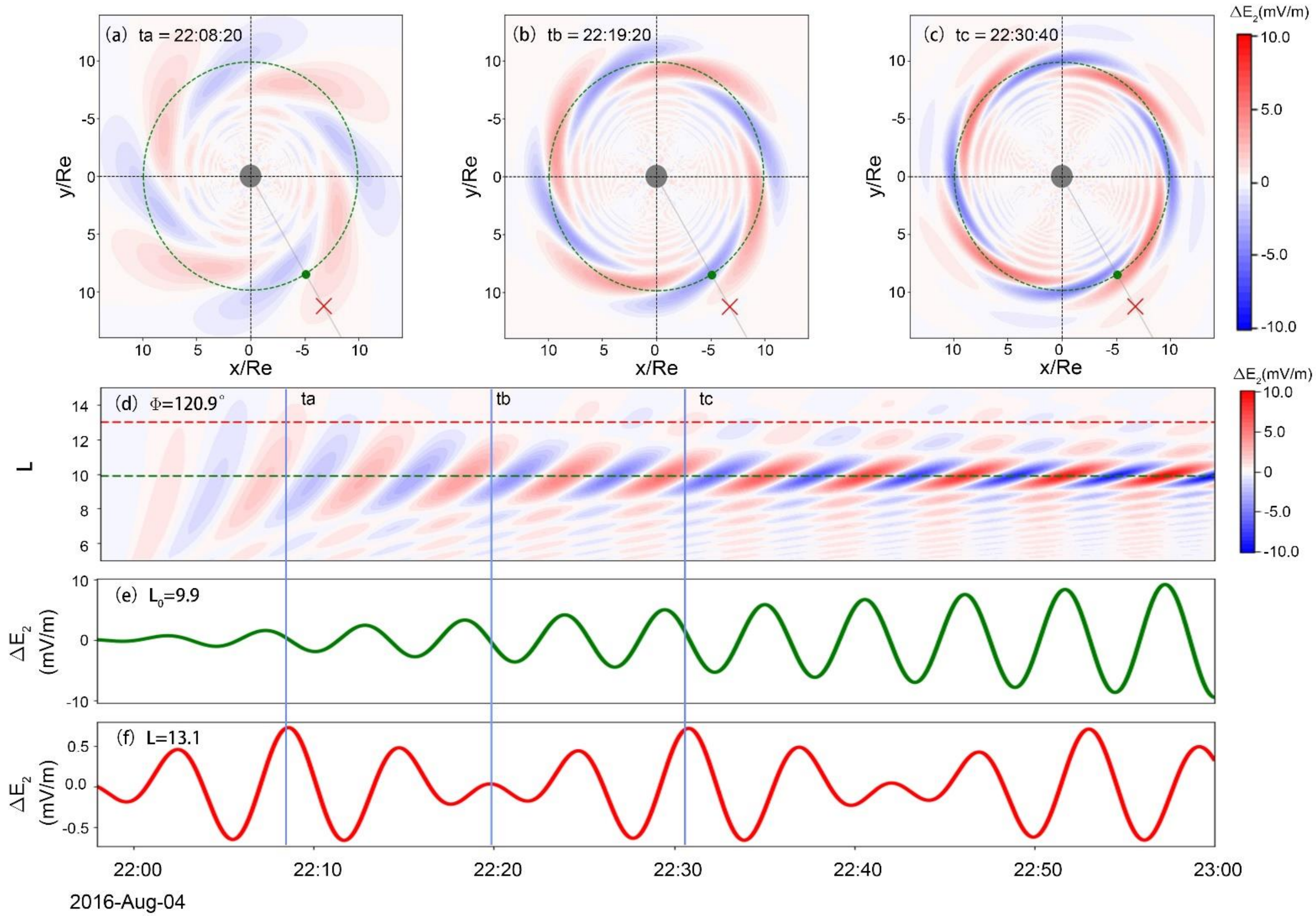

✓ **The model result reveals the reason for fluctuating wave amplitude.**

➢ Particle's trajectory in the steady waves

There are two types of resonance:

- Island A: The same drift velocity as the propagation velocity of waves.
- Island B: In resonance field line.

The trajectories are closed or periodic.

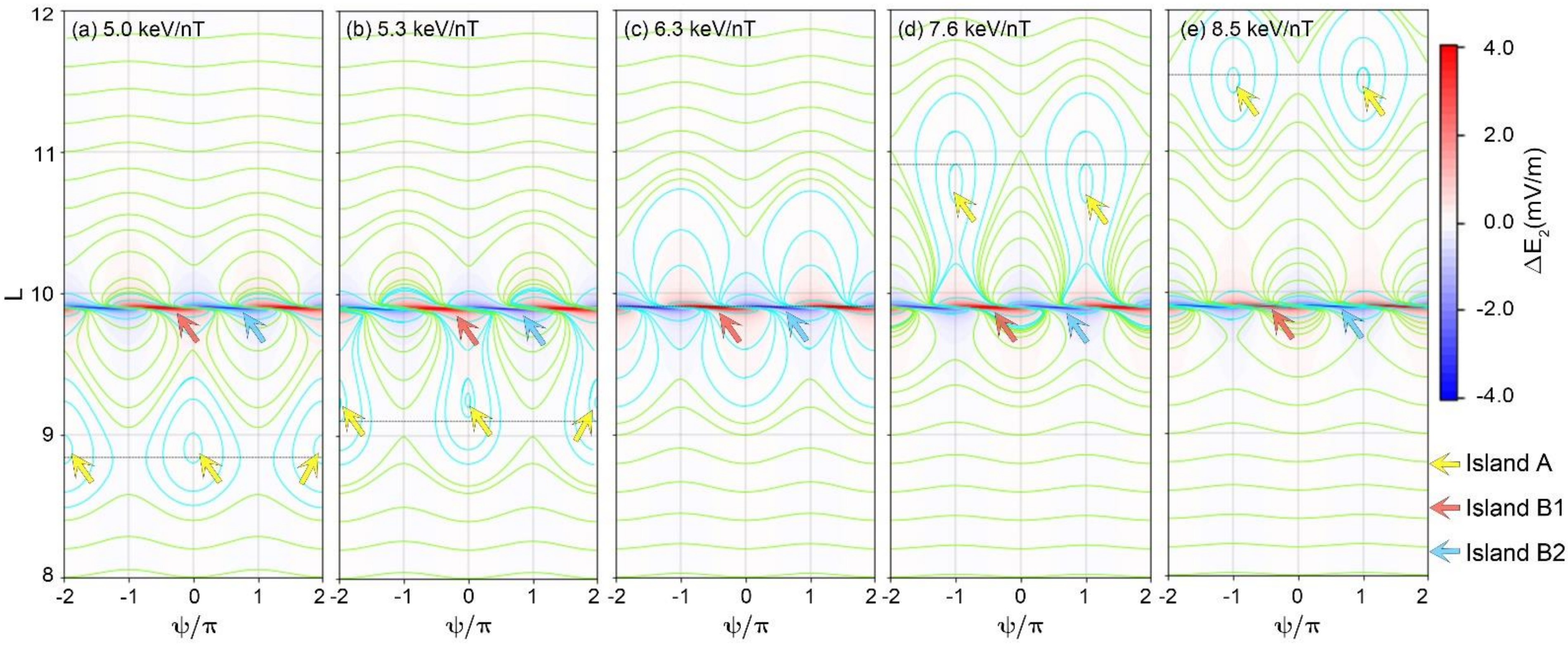

➢ Modulated flux distribution by wave

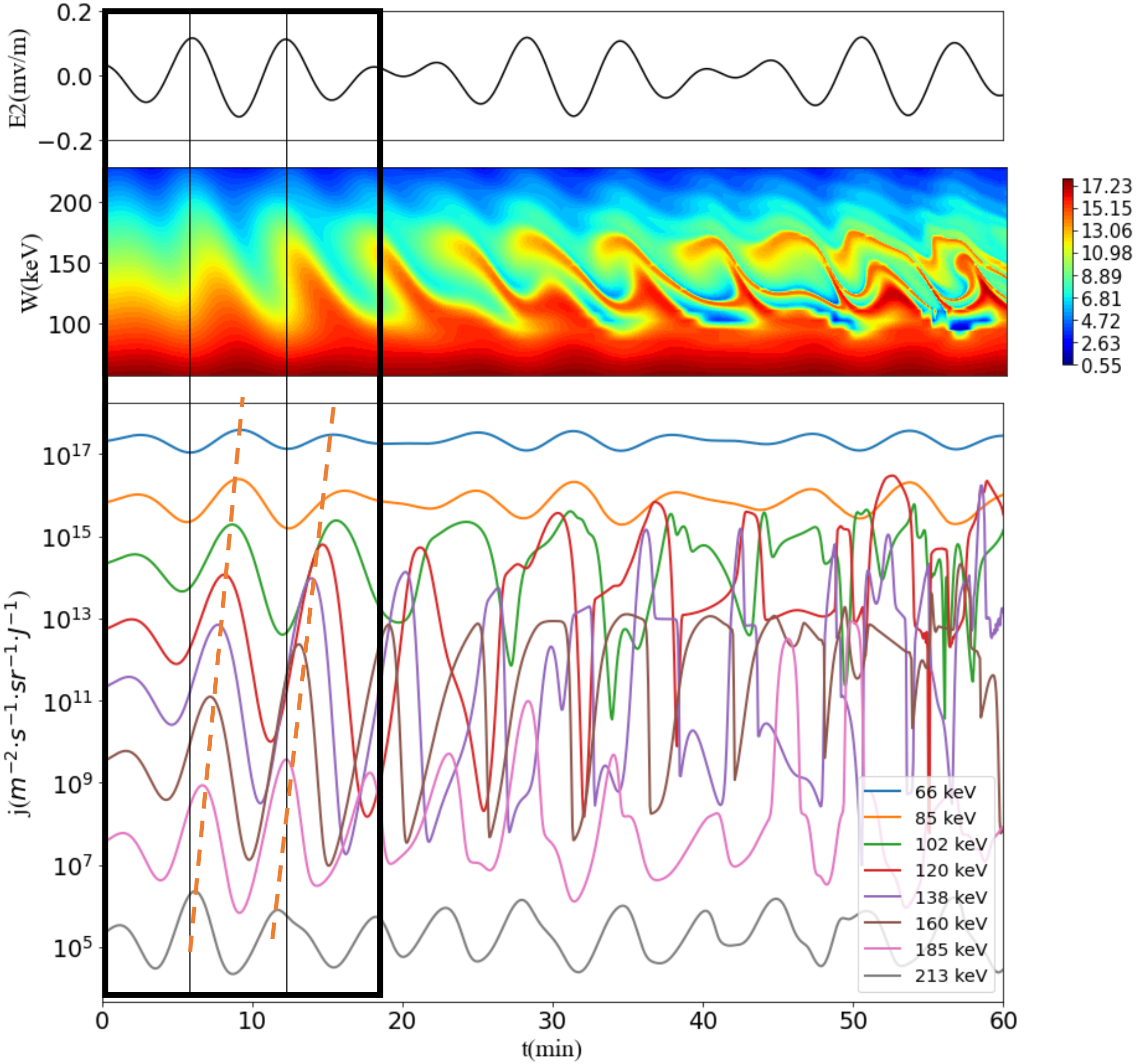

Back-trace simulation:

- Electrons with 90deg pitch angle at the equator (L=13.1).
- $\tilde{E}_{20} = 0.05\ \mathrm{mV/m}$.
- Maxwellian distribution with T = 5keV.

According to the simulation results: In the initial stages, it's clear that fluctuations of flux at different energy channels are not in-phase:

✓ higher energy and lower energy channels have the same and reverse phase with the electric field, respectively.

✓ 90 deg delay at resonance energy.

This suggests that the dynamics adhere to the drift-resonance theory

➢ Modulated flux distribution by wave

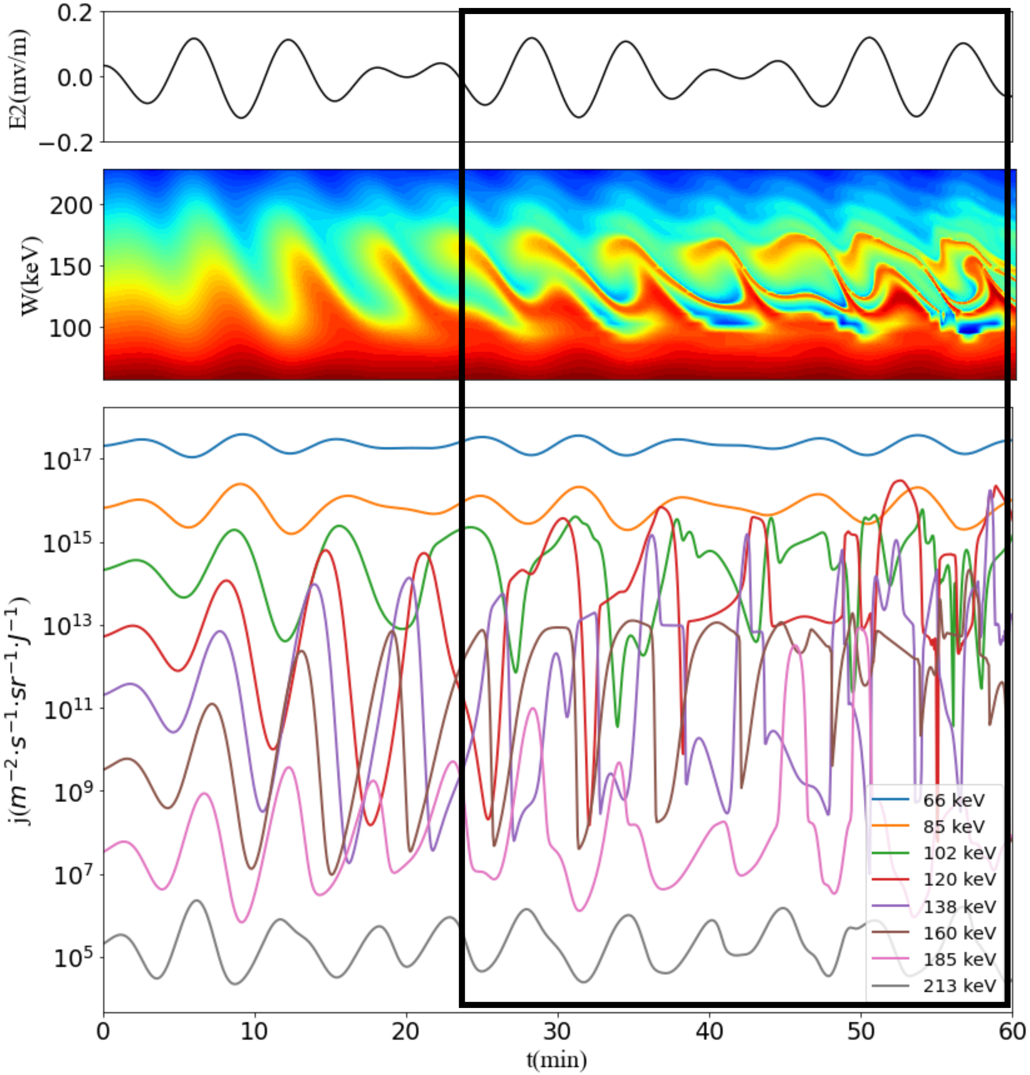

- ✓ Following linear phase of electron dynamics at the initial stages, rolled-up structures emerge in the flux spectrum as the interaction becomes non-linear.
- ✓ In the line graph of the flux, this rolled-up structure manifests as some peaks near the resonant energy channel breaking into a double-peaked pattern.

Discussion of rolled-up structures

- ✓ This aspect was not explicitly mentioned by Luo et al. (2022).
- ✓ As described in Degeling et al. (2019) the effect of a nearby FLR is to introduce additional drift-resonance locations with associated resonance islands centered on the FLR , and embedded in the original (zeroth order) drift-resonance island. The sense of vibration of trapped particles around these additional drift-resonances can be either clockwise or anti-clockwise in phase space, and leads to both clockwise and anti-clockwise rolled up structures.

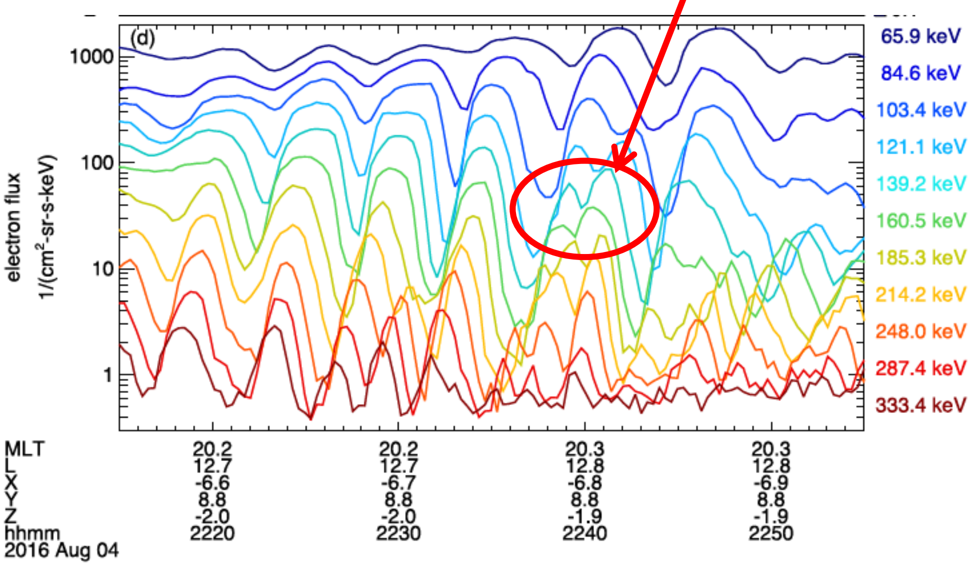

(*Luo et al., GRL, 2022*)

Summary

In this study, using an analytical model for toroidal mode:

- ✓ we were able to reproduce the B and E field of a toroidal mode event observed by the MMS mission and found that the field components of the toroidal mode from the model can fit well with the observation.
- ✓ The model shows the similar beat pattern of the field as the observation. The model reveals that the fluctuation of wave amplitude is caused by phase mixing.
- ✓ Through test particle simulations, we found that the simulated electron fluxes also displayed a similar main feature to the observations.

➢ Test particle simulation

- E&B Field: dipole field + our analytical model

$$\vec{B}(\vec{r}) = -\frac{k_0}{r^3}\left(2\cos\theta\cdot\hat{e}_r + \sin\theta\cdot\hat{e}_\theta\right)$$

- Particle motion: guiding center

$$\vec{v} = \vec{v}_{EXB} + \vec{v}_{\nabla} + \vec{v}_R + \vec{v}_{\parallel}$$

$$\begin{cases} \vec{v}_{EXB} = \dfrac{\vec{E}\times\vec{B}}{B^2} \\ \vec{v}_{\nabla} = \dfrac{\mu}{qB^2}\left(\vec{B}\times\nabla B\right) \\ \vec{v}_R == \dfrac{m v_{\parallel}{}^2}{qB^2}\left(\vec{B}\times\dfrac{d\hat{b}}{ds}\right) \\ v_{\parallel} = \dfrac{\vec{v}\cdot\vec{B}}{B} \\ \dfrac{dv_{\parallel}}{dt} = \dfrac{q\vec{E}\cdot\vec{B}}{B} - \dfrac{\mu}{m}\dfrac{dB}{ds} + m v_{\parallel}\vec{E}\times\vec{B}\cdot\dfrac{d\vec{B}}{ds} \end{cases}$$

- Distribution of particles:
  - Liouville's theorem
  - Maxwellian distribution.

➢ Dipole coordinate system

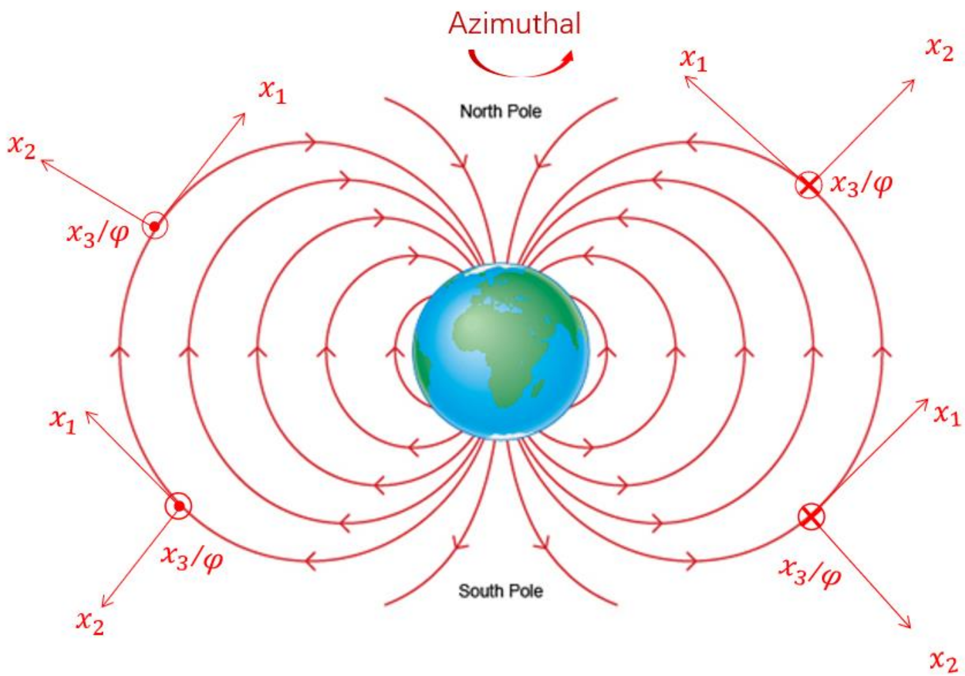

$$x_1 = \frac{\cos\theta}{r^2}, x_2 = -\frac{\sin^2\theta}{r}, x_3 = \Phi$$

The associated scale factors:

$$h_1 = \frac{r^3}{\sqrt{1+3\cos^2\theta}}$$

$$h_2 = \frac{r^2}{\sin\theta\sqrt{1+3\cos^2\theta}}$$

$$h_3 = r\sin\theta$$

Toroidal mode

E_2: the perturbed electric field in the radial direction
B_3: the perturbed magnetic field in the azimuthal direction
B_{11}: the perturbed magnetic field in the background field direction

Appendix: Analytical model

➢ Equations for ULF waves

For the idea MHD equations:

$$\begin{cases} \nabla \times \vec{E} = -\dfrac{\partial \vec{B}}{\partial t}, \nabla \times \vec{B} = \mu_0 \vec{J} + \mu_0 \varepsilon_0 \dfrac{\partial \vec{E}}{\partial t} \\ \rho_m \dfrac{\partial \vec{v}}{\partial t} = \vec{J} \times \vec{B}, \vec{E} = -\vec{v} \times \vec{B} \end{cases}$$

Toroidal mode
Construct a driven solution
with damping added

Constant Alfven speed across L:

$$V_{A0}(\square\ L_0) = C$$

$$\frac{\partial^2 h_2 E_2}{\partial t^2} + \boxed{\gamma \frac{\partial h_2 E_2}{\partial t}} - \frac{V_{A0}^{\ 2}}{r_{eq}^{\ 2}} \frac{\partial^2 h_2 E_2}{\partial s^2} = \boxed{E_{20} \omega_0^{\ 2} F(s) \cos(\omega_0 t - m\Phi)}$$

damping

driver

In general, $\gamma^2 \ \square\ \omega_0^{\ 2}$

Appendix: Analytical model

➢ The initial and boundary conditions

1. At the beginning, the E and B field are unperturbed

$$E_2\left(t=0\right)=0, B_3\left(t=0\right)=0, B_{11}\left(t=0\right)=0$$

2. No averaged perturbed field during the steady state:

$$\left\langle B_3\left(t \gg 0\right)\right\rangle_{T_{wave}} = 0$$

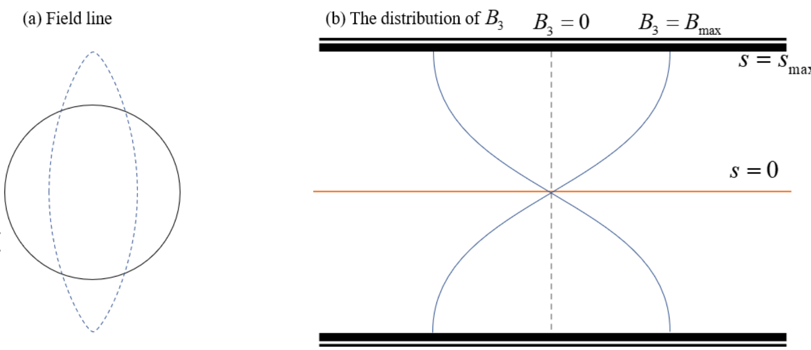

The diagram of the toroidal fundamental mode.

3. For fundamental toroidal mode:

$$B_3\left(s=0\right)=0, B_3\left(s=s_{\max}\right)=B_{\max}$$

➢ Equations for ULF waves

$$\frac{\partial^2 h_2 E_2}{\partial t^2} + \gamma \frac{\partial h_2 E_2}{\partial t} - \frac{{V_{A0}}^2}{{r_{eq}}^2}\frac{\partial^2 h_2 E_2}{\partial s^2} = E_{20}{\omega_0}^2 F\left(s\right)\cos\left(\omega_0 t - m\Phi\right)$$

$$B_3 = \int -\frac{1}{h_1 h_2}\frac{\partial h_2 E_2}{\partial x_1} dt, B_{11} = \int \frac{1}{h_2 h_3}\frac{\partial h_2 E_2}{\partial x_3} dt$$

$E_2 = ?$

$B_3 = ?$

$B_{11} = ?$

Appendix: Analytical model

➢ Analytical solution for the toroidal fundamental mode

$$E_2 = \tilde{E}_{20}\frac{(\omega_0 L_0 R_E)^2}{h_2\Delta}\cos(f_N s)\cdot\left\{\left(\omega_N{}^2-\omega_0{}^2\right)\cos(\omega_0\tau)+\omega_0\gamma\sin(\omega_0\tau)-e^{-\frac{\gamma t}{2}}\left[\Lambda\cdot\cos(\Gamma t)+\Sigma\cdot\sin(\Gamma t)\right]\right\}$$

$$B_3 = \tilde{E}_{20}\frac{(\omega_0 L_0 R_E)^2}{r_{eq}{}^2 h_3\Delta} f_N\sin(f_N s)\cdot\left\{\begin{array}{l}\dfrac{\left(\omega_N{}^2-\omega_0{}^2\right)}{\omega_0}\sin(\omega_0\tau)-\gamma\cos(\omega_0\tau)\\ -\dfrac{1}{2\omega_N{}^2}e^{-\frac{\gamma t}{2}}\left[(2\Gamma\Lambda-\gamma\Sigma)\sin(\Gamma t)-(\gamma\Lambda+2\Gamma\Sigma)\cos(\Gamma t)\right]\end{array}\right\}$$

$$B_{11} = -\tilde{E}_{20} m\frac{(\omega_0 L_0 R_E)^2}{h_1\Delta}\cos(f_N s)\cdot\left\{\begin{array}{l}\dfrac{\left(\omega_N{}^2-\omega_0{}^2\right)}{\omega_0}\cos(\omega_0\tau)+\gamma\sin(\omega_0\tau)\\ +\left[\dfrac{\left(\gamma^2-2\omega_N{}^2+2\omega_0{}^2\right)}{2\Gamma}\sin(m\Phi)-\dfrac{\gamma\left(\omega_N{}^2+\omega_0{}^2\right)}{2\Gamma\omega_0}\cos(m\Phi)\right]\sin(\Gamma t)e^{-\frac{\gamma t}{2}}\\ +\left[\gamma\sin(m\Phi)-\dfrac{\left(\omega_N{}^2-\omega_0{}^2\right)}{\omega_0}\cos(m\Phi)\right]\cos(\Gamma t)e^{-\frac{\gamma t}{2}}\end{array}\right\}$$

All symbols in the model are summarized into:

$$\left\{\begin{array}{l}\tau = t-\dfrac{m\Phi}{\omega_0}, V_{A0}=\dfrac{2\omega_0 L_0 \mathrm{R}_E\sqrt{1-1/L_0}}{\pi}, f_N=\dfrac{\pi}{2}\cdot\sqrt{\dfrac{L}{L-1}}, \omega_N=\dfrac{V_{A0}f_N}{r_{eq}}\\ s=\cos\theta, \Delta=\left(\omega_N{}^2-\omega_0{}^2\right)^2+\gamma^2\omega_0{}^2, \Gamma=\sqrt{\omega_N{}^2-\gamma^2/4}\\ \Lambda=\left(\omega_N{}^2-\omega_0{}^2\right)\cos(m\Phi)-\omega_0\gamma\sin(m\Phi)\\ \Sigma=\dfrac{2\omega_N{}^2\left(\omega_N{}^2-\omega_0{}^2\right)+\omega_0{}^2\gamma^2}{2\Gamma\omega_0}\sin(m\Phi)+\dfrac{\gamma\left(\omega_N{}^2+\omega_0{}^2\right)}{2\Gamma}\cos(m\Phi)\end{array}\right.$$

Appendix: Analytical model

- **Analytical solution for the toroidal fundamental mode**

steady state part transient part

Easy mode

$$E_2(\vec{r},t) \square \tilde{E}_{20}\frac{1}{h_2\Delta}\cos(f_N s)\cdot\left\{[\ \ ]\cos(\omega_0\tau)+[\ \ ]e^{-\frac{\gamma t}{2}}\right\}$$

$$B_3(\vec{r},t) \square \tilde{E}_{20}\frac{1}{r_{eq}{}^2 h_3\Delta} f_N \sin(f_N s)\cdot\left\{[\ \ ]\sin(\omega_0\tau)+[\ \ ]e^{-\frac{\gamma t}{2}}\right\}$$

$$B_{11}(\vec{r},t) \square -\tilde{E}_{20}m\frac{1}{h_1\Delta}\cos(f_N s)\cdot\left\{[\ \ ]\cos(\omega_0\tau)+[\ \ ]e^{-\frac{\gamma t}{2}}\right\}$$

$$f_N = \frac{\pi}{2}\cdot\sqrt{\frac{L}{L-1}}$$

$$s = \cos\theta$$

Six paraments to reproduce the wave field.

1) Frequency of monochromatic driver: ω_0
2) Wave number in azimuthal direction: m
3) Resonance field line: L_0
4) Amplitude of E in the resonance point at the equator: $\tilde{E}_{20}$
5) Damping rate of waves: γ
6) The initial time: t_0

Magnetometer observations

➢ Ground observation from CARISMA

- By the wave amplitude and wave phase along the Churchill line and Alberta line, the resonance field line should be about L=7.8. However, because the MLT of Churchill line was at about 15h-16h during the event, this value will be stretched to outward at 20MLT.
- According to the phase difference, we get the wave number should be about 3.

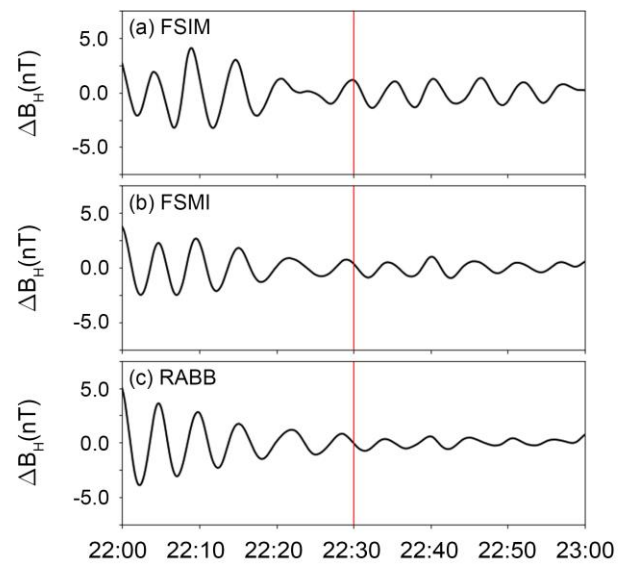

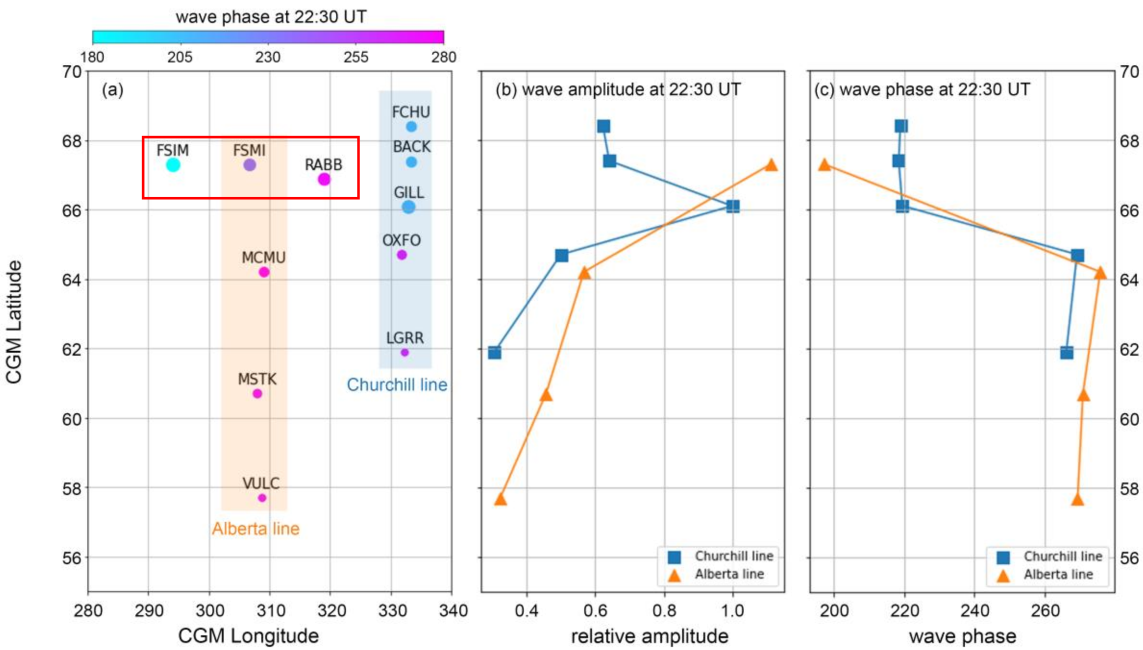

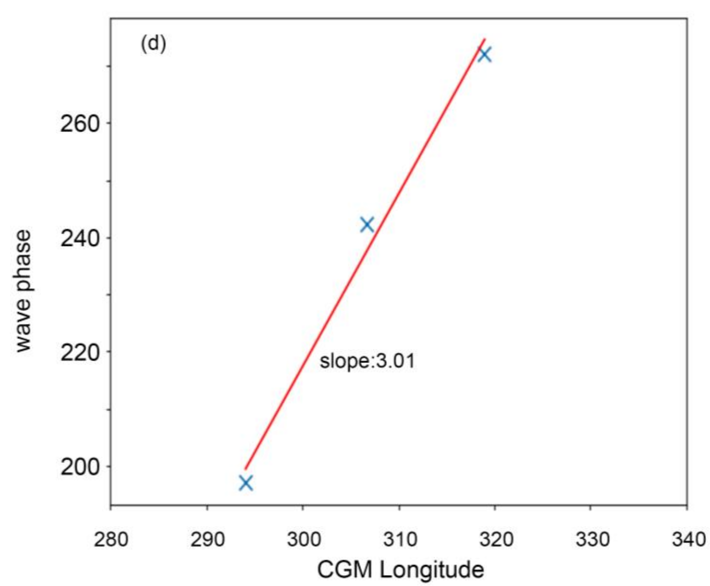

➢ Modulated flux distribution by wave

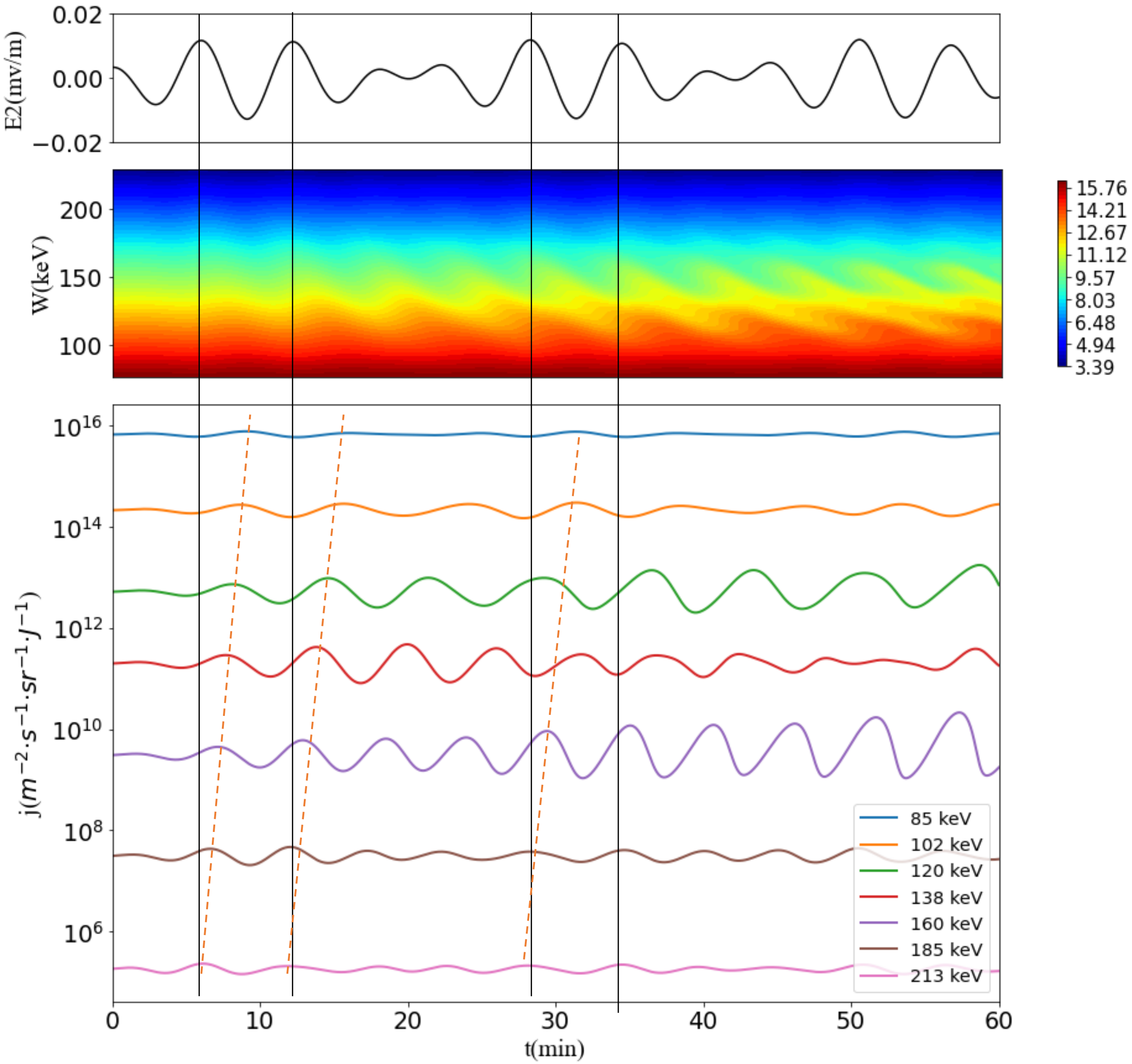

Back-trace simulation:

- Electrons with 90deg pitch angle at the equator (L=13.1).
- $\tilde{E}_{20} = 0.005\ \mathrm{mV/m}$.
- Maxwellian distribution with T = 5keV.

According to the simulation results: it's clear that fluctuations of flux for different energy channels are not in-phase:

✓ higher energy and lower energy channels have the same and reverse phase with the electric field, respectively.

✓ 90 deg delay at resonance energy.

4. Particle dynamics in the waves

➢ Modulated flux distribution by wave

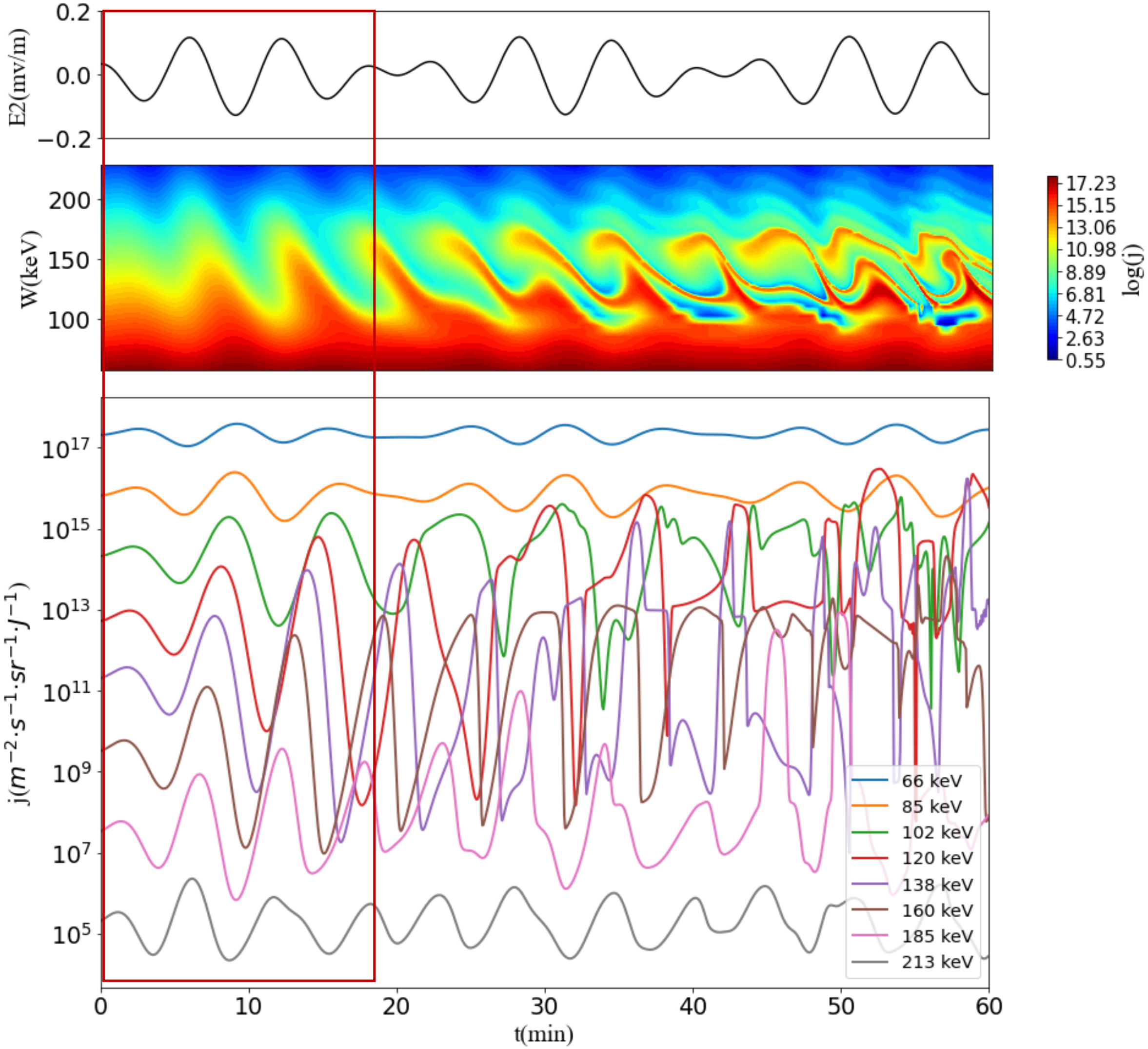

Using a larger amplitude of wave: $\tilde{E}_{20} = 0.05$ mV/m.:

✓ A larger $\tilde{E}_{20}$ leads to a greater amplitude of the flux and extends over a wider energy range.

✓ In the initial stages, the phase difference continues to adhere to the drift-resonance theory.

✓ In the later stages, a rolled-up structure emerges in the flux spectrum.